Development of a β-cyclodextrin-chitosan polymer as active coating for cellulosic surfaces and capturing of microcystin-LR

Diego Gomez-Maldonado [a], Ilari Filpponen [b], Iris B. Vega Erramuspe [a], Leena-Sisko Johansson [c], María Fernanda Mori [d], Ramapuram Jayachandra Babu [e], Matthew N. Waters [f], Maria S. Peresin [a] *

[a] Forest Products Development Center; College of Forestry, Wildlife and Environment, Auburn University. 602 Duncan Drive, 36849, Auburn. Alabama, USA
[b] Department of Chemical Engineering, Alabama Center for Paper and Bioresource Engineering (AC-PABE), Auburn University, Auburn, Alabama 36849, USA
[c] Department of Bioprocesses and Biosystems, School of Chemical Engineering, Aalto University, Aalto FI-00076, Finland
[d] Instituto de Investigaciones en Catálisis y Petroquímica, CONICET, Facultad de Ingeniería Química, Universidad Nacional del Litoral, Santiago del Estero 2829, S3000AOM Santa Fe, Argentina
[e] Harrison School of Pharmacy, Auburn University, Auburn, AL 36849, United States
[f] Department of Crop, Soil and Environmental Sciences, Auburn University, Auburn, Alabama 36849, USA

*E-mail address: soledad.peresin@auburn.edu

***Statistical Summary*:** This article has 10053 word, 8 Figures and 1 Table. There is also 1 Table and 2 Figures as supplementary information.

Abstract

In the search for more environmentally friendly adsorbent materials, the use of polysaccharides results attractive. Especially, as they can be used as coatings to add functionality to common materials as a new avenue to explore. Their inherent tendency to adsorb into each other is valuable as it adds a variety of functional groups on the outmost surface layer. Our project focuses on the pre-modification of the bio-polymer chitosan (Ch) with a 2,2,6,6-Tetramethylpiperidine-1-oxyl (TEMPO) oxidized β-cyclodextrin (Ch-TOCD), which was then adsorbed onto the cellulose nanofibrils (CNF) surface. Furthermore, the mechanism driving the adsorption of the modified chitosan onto the cellulose backbone was studied by using three different Ch-TOCD conjugates possessing different degrees of substitutions. This was conducted to evaluate whether the adsorption was guided by the change of the available electrostatic interactions between the amino (Ch) and the residual carboxyl groups of cellulose or if the adsorption was driven by the dispersive forces of the hydroxyl groups from both polysaccharides. Finally, to assess the viability of the added hydrophobic cavities (Ch-TOCD conjugate), the capture of an amphipathic toxin categorized as a monitored pollutant (microcystin-LR) was followed by Quartz Crystal Microbalance with Dissipation monitoring (QCM-D) on a surface level and by High-performance liquid

chromatography (HPLC) when the Ch-TOCD coating was applied in CNF beads. Results showed that the adsorption of Ch-TOCD was accomplished at similar levels independent of the degree of substitution. The highest adsorbed amounts of microcystin-LR were 20.5 mg/g on the model coated CNF surface, and 2.36 mg/g on the CNF coated beads. The successful coating of two nanocellulose systems and the positive adsorption of the microcystin suggest a broad-scale application of this bio-based, low energy input coating in high-end fields such as drug delivery, textile, and water restoration.

Keywords: *Active coatings, model surfaces, cellulose beads, water remediation, physical adsorption, green chemistry.*

1. Introduction

Active coatings are a novel approach to modifying surfaces by adding a specific functionality to existing materials without disrupting their bulk composition and modifying the interactions of the surface-medium interphase[1]. This added functionality can provide catalytic power to the material [2,3], stabilize it from oxidation [4], moisture [4–6], heat [7], or UV exposure [6,8]; or increase adhesion and bonding of other molecules [8–10] or cells [11,12]. It is an enhanced adsorption of the molecules that is needed when looking into water treatment, as the capacity of the material to remove pollutants is linked to its surface interaction with the water and the different pollutants [13–17]. Therefore, a variety of surface interactions is preferred when developing new water adsorbents. These range from electrostatic charges [18,19] to hydrophobic effects [20,21], which drive most pollutants capturing onto the sorbent surfaces.

The development of an active coatings could enhance the activity of natural and low-cost materials, like cellulose-based filters, for applications as water treatment. Moreover, this without the need for complex processing methods to develop scaffolds, filters, or other polymers. For this, the intrinsic affinity of β-linked polysaccharides could be easily exploited as they possess the capacity to irreversibly adsorb similar glucans – such as cellulose – onto their surface via dispersive forces [22,23]. Thus, cellulose fibers can be used as scaffolds after forming larger and more complex structures, like yarns, aerogels, textiles, and more [24–27]. Among the available polysaccharides to develop the coating, chitosan is favorable as it is obtained by the partial deacetylation of chitin, which is found in exoskeletons of crustaceous and fungi and known to be the second most abundant polymer in nature, after cellulose [28–30]. The structure of chitosan is a linear backbone of β-(1→4) 2-acetamido-2-

deoxy-β-D-glucose and β-(1→4) 2-amino-2-deoxy-β-D-glucose with more than 65 % of the deacetylated monomeric units. Because of the amino-functional groups in chitosan (with pKa 6.5) [31], the polymer shows a positive charge in acidic pH and brings the possibility of making polyelectrolyte complexes by self-assembly with negatively charged polyelectrolytes via electrostatic interactions [32].

Conversely, cyclodextrins are cyclic oligosaccharides formed by α-(1→4) D-glucopyranose, and, depending on the number of repeating units they have, are called α-cyclodextrin (6 monomers), β-cyclodextrin (7 monomers), or γ-cyclodextrin (8 monomers). One distinguishing property of cyclodextrins is the formation of a ring that provides a cone-shaped structure. This structure orients the hydroxyl groups at C2 and C3 in the wider extreme while allowing hydrogen bonding between them. Meanwhile, the hydroxyl groups at C6 are placed at the lower part in the exterior of the cone. This placement forms a highly hydrophobic cavity that can be used to form adsorption complexes with different molecules and pollutants [33]. Thus, making cyclodextrins a highly intriguing natural approach for the capture of pollutants from water sources. However, the low molecular weight of these oligosaccharides requires their attachment onto the surface of larger carriers to facilitate the recovery of the complex (*e.g.*, using filtration or other mechanisms such as magnetic attraction). Examples of previously studied carriers for the capture of microcystin-LR are magnetic graphene [34], porous silica [34], cellulose-cyclodextrin aerogels [35], and a decarboxylated PEI-coated polysulfone-biomass composite fiber [37]. Furthermore, additional capturing systems have been developed and tested with other target molecules; examples of these are regenerated cellulose nanofibers for toluene [38], chitosan via glutaraldehyde for methyl orange [39], iron oxide for heavy metals [40], multi-walled carbon nanotubes for biphenyls [41], carbonaceous nanofibers for phenolphthalein [42], or simply crosslinked β-cyclodextrin-based systems with larger particle size [43–45]. Unfortunately, many of these methodologies involve a chemical reaction with undistinguished hydroxyl groups of cyclodextrin, thus making the reaction not selective and with a high risk of blocking the active cavities. To overcome this problem, selective modification can be done in C6 by green processes such as TEMPO oxidation [46–48], which has recently been improved to allow neutral pH conditions instead of the traditional alkaline media, which might imply chemical degradation [49,50].

The main advantage of the neutral TEMPO-$NaClO/NaClO_2$ oxidation in aqueous media is that it allows the selective oxidation of the primary alcohol functional groups of β-cyclodextrin to carboxylic functional groups under mild conditions, which in turn allows the preparation of TEMPO-mediated β-cyclodextrin (TOCD) with low degradation rates. This further allows us to use chemistry such as *N*-ethyl-*N*'-(3-(dimethylamino)propyl) carbodiimide (EDC) and *N*-hydroxy succinimide (NHS) assisted coupling reactions. The EDC/NHS activation approach can be used to bind the carboxyl-containing TOCD to other compounds that contain amino groups such as chitosan [51–53].

As mentioned above, chitosan possesses amino functional groups that can be used as active sites for crosslinking with other molecules that have carboxyl groups *via* EDC/NHS reaction or similar chemistry. For example, Jiang *et al.* [39] used maleic anhydride and EDC to link cyclodextrin to chitosan and form a network with the chitosan molecules. Similarly, glutaraldehyde can be used to immobilize CD to chitosan before anchoring it to graphene, as described by Li *et al.* [54]. Nevertheless, in both approaches, the orientation of the CD or the use of only the amino groups is not favored. Therefore, a pretreatment such as TEMPO-mediated oxidation of CD together with selective coupling chemistry could improve the orientation of CD.

The modification of chitosan with TEMPO-oxidized β-cyclodextrin was previously done on a chitosan precoated cellulose yarn [50]. However, the present work aims to modify the homogenous solution of chitosan with TEMPO-oxidized β-cyclodextrin in different molar ratios (Ch/TOCD 1:2, 1:1, and 3:1) and measure the resulting conjugates adsorption onto the surface of cellulose nanofibrils (CNF). This will allow the comparison between the electrostatic interactions and van der Waals forces in the self-assembly. Furthermore, the developed system is used to capture microcystin-LR from an aqueous solution to mimic an active coating material that could be used for the environmental water treatment.

Microcystin-LR is a toxin that impacts human health due to its ability to promote the growth of tumors, predominantly in the liver [55,56]. The concentration of this toxin is increasing and surpassing the upper limit established by the World Health Organization (WHO) of 1 µg/L [57] in water reservoirs as a consequence of the increase in the occurrence and duration of cyanobacterial blooms [58]. Microcystins are a family of toxins composed of cyclic oligomers with seven amino acids, including the unique amino acid (2S,3S,8S,9S)-3-Amino-

9-methoxy-2,6,8-trimethyl-10-phenyldeca-4,6-dienoic acid (ADDA) at position 5. The difference between the microcystin variants is given by the substitutions in positions 2 and 4, which are leucine and arginine for the microcystin-LR [59,60]. The ADDA amino acid shared by all microcystins is highly hydrophobic due to the phenyl terminal group and the long unsaturated tail, making it an ideal target anchoring point on hydrophobic active sites. As shown by Archimandritis *et al*. [61], β-cyclodextrin (CD) can effectively capture microcystin-LR (MC), which makes it a promising molecule to assess the viability of the cavities on the active coating while targeting an emerging contaminant that is accumulating in water sources every day.

Therefore, this work aimed to generate a cyclodextrin-chitosan polymer that can form complexes with microcystin-LR and which can be used as an active coating on CNF-based films and hydrogels. To evaluate the adsorption capacity of the modified chitosan, three different conjugates of chitosan (Ch) and TEMPO-oxidized β-cyclodextrin (TOCD) were explored. Conjugates were prepared using EDC/NHS-assisted coupling chemistry with molar ratios of 1:2, 1:1, and 3:1 of the aforementioned polysaccharides, this to reach Ch-TOCDs possessing different degrees of substitution (DS) values. After chemical characterization, the adsorption of the modified chitosan derivatives was first evaluated at the surface level by Quartz Crystal Microbalance with Dissipation monitoring (QCM-D) and the capacity to remove the toxin. Finally, the best performing coating was used to coat CNF-based hydrogel beads and used to remove the toxin, while the capture kinetics was followed by High-performance liquid chromatography (HPLC).

2. Materials and methods

2.1. Materials

Bleached cellulose nanofibrils (CNF, 2.76%, pH 6.3) were produced at the Forest Products Development Center at Auburn University from bleached kraft pulp starting with mixed softwood kindly provided by a North American Mill (more information of this material can be found at [36]). β-cyclodextrin (CD, > 95 % purity) and *N*-hydroxysuccinimide (NHS, 98.0% purity) were obtained from Tokyo Chemical Industry (Portland, OR, U.S.). The utilized chitosan ($DS_{acetylation}$ of 0.15, MRU 167.3 g/mol) was purchased from Alfa Aesar (Haverhill, MA, U.S.), while sodium chlorite (80% purity) was obtained from BeanTown

159 Chemical (Hudson, NH, U.S.). Sodium hypochlorite (12.5 % w/w, 2 M in water) was bought
160 from VWR chemicals (Radnor, PA, U.S.). 2,2,6,6-tetramethylpiperidinooxy (TEMPO, 98 %
161 purity) was purchased from Acros Organics (Geel, Belgium) and 3-(3-
162 Dimethylaminopropil)-1-ethyl-carbodiimide hydrochloride (EDC, 99.9% purity) was
163 obtained from Chem-Impex International (Wood Dale, IL, U.S.). Meanwhile, polyethylene
164 glycol (PEG, Mw 10 000) and polyethylenimine, branched (PEI, Mw 25 000, Mn 10 000)
165 were obtained from Aldrich (San Luis, MO, U.S.). Microcystin-LR (MC, > 95 %) was
166 purchased from Cayman Chemicals (Ann Arbor, MI, U.S.); and sodium hydroxide (50 %
167 w/w) was purchased from J.T. Baker (Phillipsburg, NJ, U.S.). The water used was deionized
168 and purified with a Thermo Scientific Barnstead Nanopure (18.2 MΩ cm). Unless specified,
169 all the weights in this paper are expressed on oven dry basis.

170 *2.2. Synthesis of TEMPO oxidized β-cyclodextrin (TOCD)*

171 β-cyclodextrin was carboxylated by neutral TEMPO-NaClO-$NaClO_2$ oxidation in aqueous
172 media (Figure 1a) [50,62]. For this, 5 g of β-cyclodextrin was dissolved in 450 mL of sodium
173 phosphate buffer (0.05 M, pH 6.8). Then 0.08 g of TEMPO (0.1 mmol/g) and 5.65 g of
174 sodium chlorite (80 %, 10 mmol) were added to the cyclodextrin solution. Simultaneously,
175 the 2 M sodium hypochlorite was diluted to a 0.1 M in the buffer, and 23 mL of this dilution
176 was added in one step to the reactive solution to obtain a final concentration of 5 mmol
177 (1.0 mmol NaClO/g of CD). The reaction was conducted in a closed flask for 19.5 h under
178 ambient conditions and a constant stirring of 500 rpm.
179 After modification, TEMPO-oxidized β-cyclodextrin (TOCD) was purified by dialysis
180 against ultrapure water (18.2 Ω) in a 100-500 Da dialysis membrane tube, then concentrated
181 with reverse dialysis in PEG before freeze-drying.

182 *2.3. Synthesis of chitosan-cyclodextrin polymers (Ch-TOCD)*

183 The synthesis of Ch-TOCD was performed with three different molar ratios, which were
184 calculated from the functional groups (NH_2 and COOH) of the participating polysaccharides
185 (Chitosan and TEMPO-oxidized β-cyclodextrin). Molar ratios of 1:2, 1:1, and 3:1 were
186 chosen, and the syntheses were conducted (Ch/TOCD 1:2, 1:1, and 3:1) in a total volume of
187 50 mL following the same sequence of steps. A scheme of the methodology utilized is
188 presented in Figure 1b. First, the TOCD was dissolved in 1% acetic acid (125, 50, and 50 mg)
189 to obtain a final concentration of 0.05%, and then 1-ethyl-3-(3-dimethylaminopropyl)

carbodiimide (EDC) was added to a final concentration of 0.05 M of EDC. The resulting solution was stirred before adding N-hydroxysuccinimide (NHS) to obtain a final concentration of 0.2 M of NHS. Next, chitosan was added from a stock solution (1%chitosan in 1% acetic acid, w/w) to obtain 25 mg, 25 mg, and 50 mg, respectively. The reaction was stopped after 24 h by adding ethanolamine (61 µL, 0.1M). Purification and concentration were done by five cycles of washing by using 30 KDa Pall-membrane centrifugation tubes (Macrosep Advance Centrifugal Device, Pall Corporation) at 3000 rpm for 1 h.

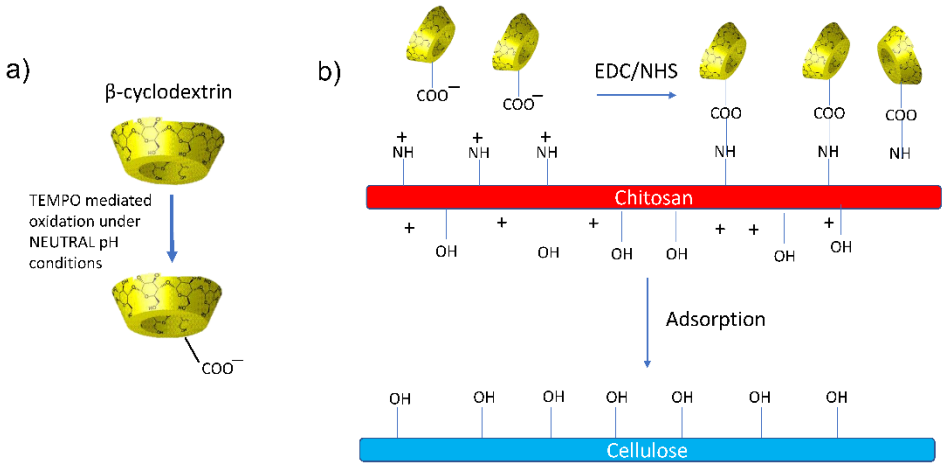

Figure 1. Scheme of the reactions used for the generation of the chitosan-g-cyclodextrin (Ch-TOCD) coating (a) TEMPO mediated oxidation of the β-cyclodextrin, and (b) grafting of the TOCD to chitosan by EDC/NHS chemistry and immobilization onto cellulosic materials by adsorption.

2.4. Nanocellulose bead generation

A 1.4% consistency cellulose nanofibril alkaline solution was generated, targeting a final concentration of 7 % w/w NaOH and 12% w/w urea mixed at -10°C with a recirculating bath. Once dissolved, the cold solution was added dropwise to 50 mL of 2 M nitric acid solution in a graduated cylinder. After 10 min in the coagulation bath, the obtained beads were transferred into a reservoir with ultrapure water and thoroughly washed under a continuous flow of ultrapure water overnight.

The coating was done by immersing the neutralized beads into a 50 mM NaOAc buffer pH 5 containing 0.05 wt.% of the chitosan or the Ch-TOCD derivatives for 24 h, followed by washing with ultrapure water until neutral pH was obtained.

The solid content was calculated by taking five wet beads and drying them in an aluminum pan at 105 °C overnight. The dry mass was obtained, and dry content was calculated by the difference between their dry and wet weight, i.e., moisture content. All measurements were done by triplicates.

2.5. Characterization techniques

TEMPO oxidized β-cyclodextrin (TOCD) titration

Degree of oxidation (DO) was determined by pH and conductivity titration methods, based on the calculations reported by da Silva Perez [63] and the standard SCAN-CM 65:02. For this, TOCD suspension was first brought to pH 3 with 10 mM HCl to assure the protonation of all present acid moieties. After freeze-drying, 30-40 mg of TOCD in acidic form were dissolved in 15 mL of 10 mM HCl and titrated with 10 mM NaOH by adding 1 mL every 5 min and measuring pH and conductivity with a VWR symphony B30PCI multiprobe conductometer. The degree of oxidation was then calculated by the following equation:

$$DO = 162(V2 - V1)c/[w - 36(V2 - V1)c] \quad (1)$$

Where V1 and V2 are the amount in L of NaOH used to reach the end points 1 and 2, respectively; c is the concentration of the base in mol L^{-1}, and w is the dry weight of the sample. V1 and V2 were determined by the second derivative of pH curve (or conductivity curve), using the volumes where the graph crossed the origin.

Fourier-transform infrared spectroscopy (FTIR)

The degree of oxidation (DO) was also estimated by FTIR spectroscopy measurements. Before the measurements, TOCD was treated with a 0.01 M HCl until a final pH of 3 was achieved to get the compound in the acid form. This eliminated the interference between the band involving the out-of-phase COO^- stretching vibration in the carboxylic salt, and the band observed due to the presence of adsorbed water (~1640 cm^{-1}) [64]. DO was then measured by calculating the ratio of the intensity of the carbonyl band (1730 cm^{-1}) to the stronger cellulose backbone band (1050 cm^{-1}). Both TOCD and Ch-TOCD samples were analyzed for characterization of KBr pellets on a PerkinElmer Spotlight 400 FT-IR Imaging System (Massachusetts, US) with a transmission accessory and a resolution of 4 cm^{-1}. First, a background spectrum was measured, which was carried out before each set of measurements with the same number of scans. To lower the noise in the spectrum bands, 128

scans per spectrum were measured by duplicates in different areas of the sensor. Data was processed with Spectrum 6 Spectroscopy Software (PerkinElmer, Massachusetts, US).

X-ray Photoelectron Spectroscopy (XPS)

Surface characterization of pure and modified chitosan powders was carried out using the AXIS Ultra DLD Photoelectron spectrometer (Kratos Analytical, Manchester, UK), under neutralization. Samples were mounted on the sample holder with UHV compatible carbon tape, together with an in-situ reference of pure cellulose [65] and pre-evacuated overnight. Surface elemental content was calculated from low-resolution wide scans, while C 1s, O 1s, and N 1s high-resolution regional spectra were utilized for more detailed chemical information. Data was collected from 2-4 locations for each sample. The data was analyzed using CasaXPS software, with the C-O component of high-resolution C 1s signal at 286.7 eV as the binding energy reference [66,67]. The spectra were fitted assuming Gaussian-Lorentzian distribution for each peak, with a Shirley background and FWHM restrictions [68].

Elemental Analysis (EA)

Freeze-dried samples were processed in an ECS 4010 Elemental Combustion System CHNS-O from Costech Analytical technologies, Inc (Firenze, Italy), and data were analyzed with the ECS60 software. Nitrogen- and Carbon content were collected and fitted into standard curves with correlations of 0.99996 and 0.99998 for N and C, respectively. C/N molar ratio is reported.

Quartz Crystal Microbalance with Dissipation Monitoring (QCM-D) measurements

The generation of the CNF surfaces, adsorption of Ch-TOCD, and capture of microcystin-LR (MC) were all studied on gold-coated quartz sensors in a QSense Analyzer from Biolin Scientific (Västra Frölunda, Sweden). The basic principle of the QCM-D is the following: changes in frequency (Hz) of a piezoelectric sensor that has a base resonance of 5 MHz, and its overtones 15, 25, 35, 45, 55 and 75 MHz are measured; the changes in the frequency resonance are proportional to the change in mass on the sensor. Because the surface is interacting with a flow of matter only, those changes are correlated to the mass adsorption on the sensors surface [69–71]. Sauerbrey [72] determined the relationship between changes in frequency and mass for rigid layers, uniformly distributed on the surface of the sensor and with lower values of mass than the mass of the crystal with the following equation:

$$\Delta m = C * \Delta F * n^{-1} \quad (2)$$

Where the constant for 5 MHz crystals (C) is equal to -17.7 ng/cm^2, ΔF is the change in frequency and n is the overtone number. Since most of the polymeric systems do not generate a rigid layer, Sauerbrey's equation underestimates the adsorbed mass; some other models have been generated to address the changes of mass, like Voigt's and Maxwell's. These models take in to account the density, and the dynamic and static viscosity of the adsorbed materials as well as the crystal's [73].

The dissipation factor ΔD is related to the viscoelastic properties of the layers formed on the crystal, as it translates the relationship of energy dissipation from the sensor to the fluid and the energy stored (3); it can be measured as it is inversely proportional to the decay time constant (τ) and the resonant frequency (f) as it is shown in equation 4 [73].

$$D = \frac{E_{dissipated}}{2\pi E_{stored}} \quad (3)$$

$$D = \frac{1}{\pi f \tau} \quad (4)$$

If the generated film is viscous, energy is dissipated due to the oscillation of the layer; more energy is lost and longer decay times are present which translates to a decrement in the D factor [74]. When more energy is stored, as the surface is being rigidize, increments in the D-factor will be observable [74].

All measurements were made at 25 °C with a constant flow of 100 µL/min on gold coated crystals. First, a 0.1 % (m/v) solution of PEI was passed as anchoring solution, followed by a 0.1 % (m/v) CNF solution to cover the sensor and form 2-D model films. For the chitosan-cyclodextrin polymers, a concentration of 0.5 mg/mL was used in a 50 mM NaOAc buffer at pH 5, and 50-mM ionic strength adjusted with NaCl; and 10 µg/mL of microcystin-LR in the same buffer. Only the changes of the third overtone are presented to make the figures explicit. Mass was calculated using the Broadfit model (based on the Voight model) with dissipation dependency from frequency changes, this at the DFind Software from Biolin Scientific (Västra Frölunda, Sweden); densities were 1030, 1200, 1770, and 1299 g L^{-1} respectively for PEI, CNF, chitosan, its derivatives, and Microcystin-LR.

Gold crystals were previously cleaned with NH_4OH, H_2O, H_2O_2 hot solution (at ratio of 5:1:1, w/w) at 60 °C for 15 min, followed by 15 min in ultrapure water, and 1 min in piranha

300 solution (at ratio of 3:1, w/w of H_2SO_4 and H_2O_2, respectively) with abundant rinsing and 30
301 min in Novascan PSD Series Digital UV Ozone System (Iowa, US).
302 **High Performance Liquid Chromatography (HPLC)**
303 For the analysis of microcystin, the EPA method 544 was adapted. Briefly, ca. 200 mg of
304 swollen uncoated and coated bead were placed in 10 mL of solutions containing 6.5 µg/mL
305 at room temperature and constant stirring. 150 µL aliquots were taken at the corresponding
306 time and analyzed in a Waters Alliance HPLC (Model No. e2695, Waters Corp., Milford,
307 MA, USA) system equipped with a solvent management system 2695 and detected by a
308 photodiode array detector (PDA, 2998). The system also counts with a thermostatically
309 controlled column compartment and an autosampler. The method used was adapted from the
310 one described by Meriluoto & Codd [60]. Briefly, a C-18 column (55x4 mm) was used as
311 stationary phase, and 0.05 % trifluoroacetic acid (TFA) aqueous solution/0.05 % TFA
312 acetonitrile with linear gradient at a flow rate of 1 mL/min, and 10 µL injections using the
313 autosampler in cycles of 9 min. The retention time was 4.2 min and correlation of the samples
314 to the standard curve was of 0.9997. All experiments were done by duplicates and averaged.
315 The analysis of the data was performed using Empower® 3 software (Waters Corp., Milford,
316 MA, USA).
317 **Kinetics.**
318 The fitting of the data to calculate rate constants (k_2) and adsorbed amounts in equilibrium
319 (q_e) was done for a pseudo-first order and pseudo-second order models when possible,
320 following the equations given in by Tran et al. [30]. Briefly, for pseudo-second order:

$$\frac{t}{qt} = \frac{1}{h} + \frac{t}{qe} \quad (5)$$

321 where $h = k_2 q_e^2$, and k_2 being the pseudo-second order rate constant of sorption, respectively.
322 q_e is the amount of analyte adsorbed at equilibrium (mg/g), and qt is the amount of analyte
323 adsorbed at any time (mg/g).

324 3. Results and discussion

325 *3.1. TEMPO-mediated oxidation of β-cyclodextrin*

326 The modification of the β-cyclodextrin was confirmed by the presence of the band
327 corresponding to the carboxyl group (1740 cm^{-1}) installed during the TEMPO mediated

oxidation (Figure 2b and Figure S1). Likewise, the FTIR (Figure S1) did not show signals in the C-H region that could correspond to aldehyde formation, suggesting that the selection of the milder reaction with TEMPO at neutral pH conditions helped to retain the structure of the cyclodextrin, and therefore its capacity to capture molecules [50]. Moreover, the increase in the signal at 1650 cm^{-1} likely relates to the O-H bending of the installed COOH groups which is in agreement with the previous studies [50,75].

To investigate the degree of oxidation (DO) of the β-cyclodextrin, the inflexions points found in the pH titration graph presented in Figure 2a were used to identify the point in which the functional groups reached a pKa point. Such inflexion points were observed between the volumes 14 and 16 mL for the first point, and 20 and 24 mL in the different repetitions: giving an averaged DO of 0.29. Considering that only C6 in the glucose monomer is reactive in the TEMPO-mediated oxidation reaction, the maximum DO possible equals to 1 [76]. Therefore, 0.29 is approximate two sevenths of it, indicating the modification of at least one C6 in each β-CD. This selective modification would ideally help in the further grafting of the chitosan, as it would assure that C6 is the carbon interacting with the polymers, thus leaving the cavity exposed to capture the pollutant and avoiding the closure of the cavity by random immobilization.

(a)

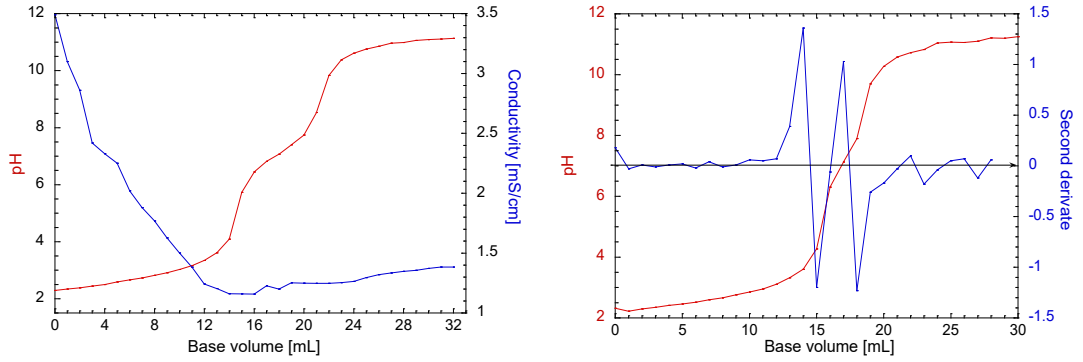

(b)

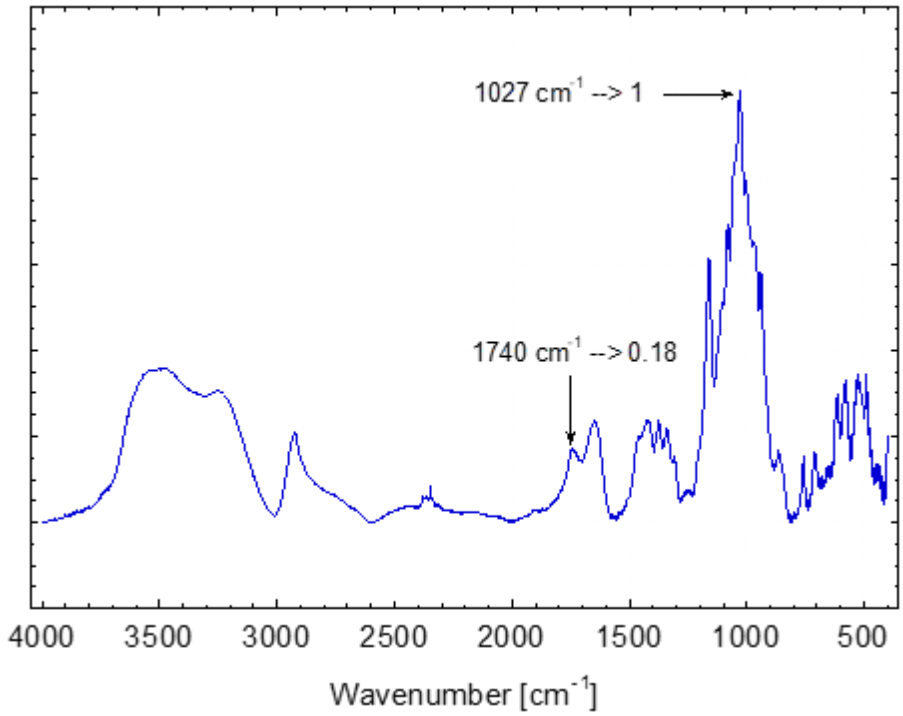

Figure 2. (a) Conductivity and pH titration of TEMPO oxidized beta-cyclodextrin (left) and determination of inflexion points for volumes determination (right). (b) FT-IR spectrum (KBr method) of the TEMPO-mediated oxidized beta-cyclodextrin showing the carbonyl band (1740 cm^{-1}) and C-O stretching (1027 cm^{-1}).

FTIR spectrum in Figure 2b displays a shift in the C-O stretching band, which is traditionally found at 1050 $cm^{-1}$to 1027 cm^{-1}. This shift is suggested to be derive from the cyclic structure as observed for other cyclodextrin spectra [75]. Moreover, the ratio of this band and the carbonyl band (1740 cm^{-1}) after normalization and baseline correction was found to be 0.18, which in turn means that approximately one to two of the seven monomeric units of β-cyclodextrin are oxidized [77]. This result is in agreement with the titration results and with the previously presented theory of the maximum amount of accessible monomeric units (3) of β-cyclodextrin before the possible steric hindering starts to appear [46].

As titration is considered more accurate method for the determination of the degree of oxidation, several repetitions were performed with similar results, confirming this modification even between different batches.

3.2. TOCD grafting to chitosan.

To assure the successful modification of chitosan, elemental analysis, FTIR, and XPS measurements were performed. In Table 1, the percentages of C and N are presented as well as the C:N ratio, which was used to calculate the degree of substitution (DS) values for chitosan and Ch-TOCD conjugates. It is worth mentioning that the maximum DS for the conjugates is 0.85 as the deacetylation degree of chitosan is 0.85. Ch-TOCD 1:2 displays the highest DS of 0.57, while the Ch-TOCD 1:1 and Ch-TOCD 3:1 have similar DS values of 0.28 and 0.30, respectively. The similarity of the DS of the Ch-TOCD 3:1 and 1:1 could be related to the lower concentration (in relation to Ch) of TOCD used, which could have hindered the coupling efficiency.

Table 1. Elemental Analysis of Chitosan derivatives and Degree of substitution estimation.

	%C	%N	C/N	DS
Chitosan	40.38	7.35	6.41 ± 0.01	0.03
Ch-TOCD 3:1 (NH_2: COOH)	39.91	5.95	7.81 ± 0.1	0.30
Ch-TOCD 1:1 (NH_2: COOH)	40.03	6.27	7.44 ± 0.3	0.28
Ch-TOCD 1:2 (NH_2: COOH)	40.05	5.22	8.95 ± 0.4	0.57

XPS was used to verify the modification of amine groups of the chitosan. The results of the wide energy region spectra, the high-resolution C1 and N1 are shown in Figure 3 and their atomic concentration percentages, carbon/nitrogen (C/N) ratio, and signal locations are summarized in Table S1 (Please see SI). Overall, three signals were present in the modified materials, the one corresponding to carbon centered at 286.7 eV, a nitrogen signal centered at 401 eV, and the oxygen centered at 533 eV. When the percentage of the elements was calculated, the first indication of the modification was the shift from the original 60.0% C of the chitosan. In the case of the Ch-TOCD 3:1, the C decreased to 58.3%, while the other 2 conjugates (Ch-TOCD 1:1 and Ch-TOCD 1:2) showed increases of 68.0% and 67.8%, respectively. Conversely, the N% decreased as the content of cyclodextrin increased, from 7.7% of the pure chitosan to 7.1% for the Ch-TOCD 3:1, 6.3% for Ch-TOCD 1:1, and as low as 3.0% for Ch-TOCD 1:2. It should be noted here that the above trend has been seen in other systems using EDC/NHS chemistry for crosslinking [78].

386 The close observation of the carbon in the high-resolution plots revealed that the carbon
387 signal was deconvoluted into 4 clear peaks. The C-H and C-C show at 285±0.2 eV with a
388 slight shift to higher energy when the C-N was present [65]. An increase of signal can be
389 mainly observed for the pure chitosan when compared to the cellulose reference and for the
390 conjugates as new C-C and C-H are added as the amount of cyclodextrin increases. However,
391 the C-N signal is traditionally located at 286.1 ± 0.1 eV [79], which overlaps with the C-O
392 signal when the nitrogen becomes more surrounded by oxygen as is the case while the amount
393 of cyclodextrin is increased. Therefore, at 286.7 eV the C-O peak was observed with a more
394 defined peak as the number of crosslinking increased. The signal related to O-C-O was found
395 at 288.1 ± 0.1 eV, and the signal corresponding to O-C=O was located at 289.1± 0.05 eV.
396 Meanwhile, the high-resolution N1s plot showed two define signals, one at 399.8 ± 0.1 eV
397 from the unmodified amine groups [80] and the second for formed OC-NH bonds at 402.1 ±
398 0.1 eV [78,81]. Here, the Ch-TOCD 1:2 presented lower relative values of N% while
399 compared with the other two conjugates, suggesting that the additional C% in the sample can
400 be attributed to the presence of the cyclodextrins. Moreover, when the rations of the coupled
401 nitrogen (OC-NH) against the amino groups (N-H), are compared, a larger contribution of N
402 species is seen for the Ch-TOCD 1:2 than for the other two conjugates (Table S1).
403 To get a better perspective of the modification, the C/N ratio (Table S1) was also calculated
404 similarly to the elemental analysis presented above (Table 1). There a greater difference
405 between the derivatives was calculated, with the Ch-TOCD 1:2 having 2.1x and 2.8x higher
406 ratios than the 1:1 and 1:3, respectively, and 2.9x higher that the pure chitosan. This further
407 confirms the higher presence of cyclodextrin -and their C- for the 1:2 derivative, which is
408 also present and exposed in generated surfaces and should be available for the generation of
409 inclusion complexes.

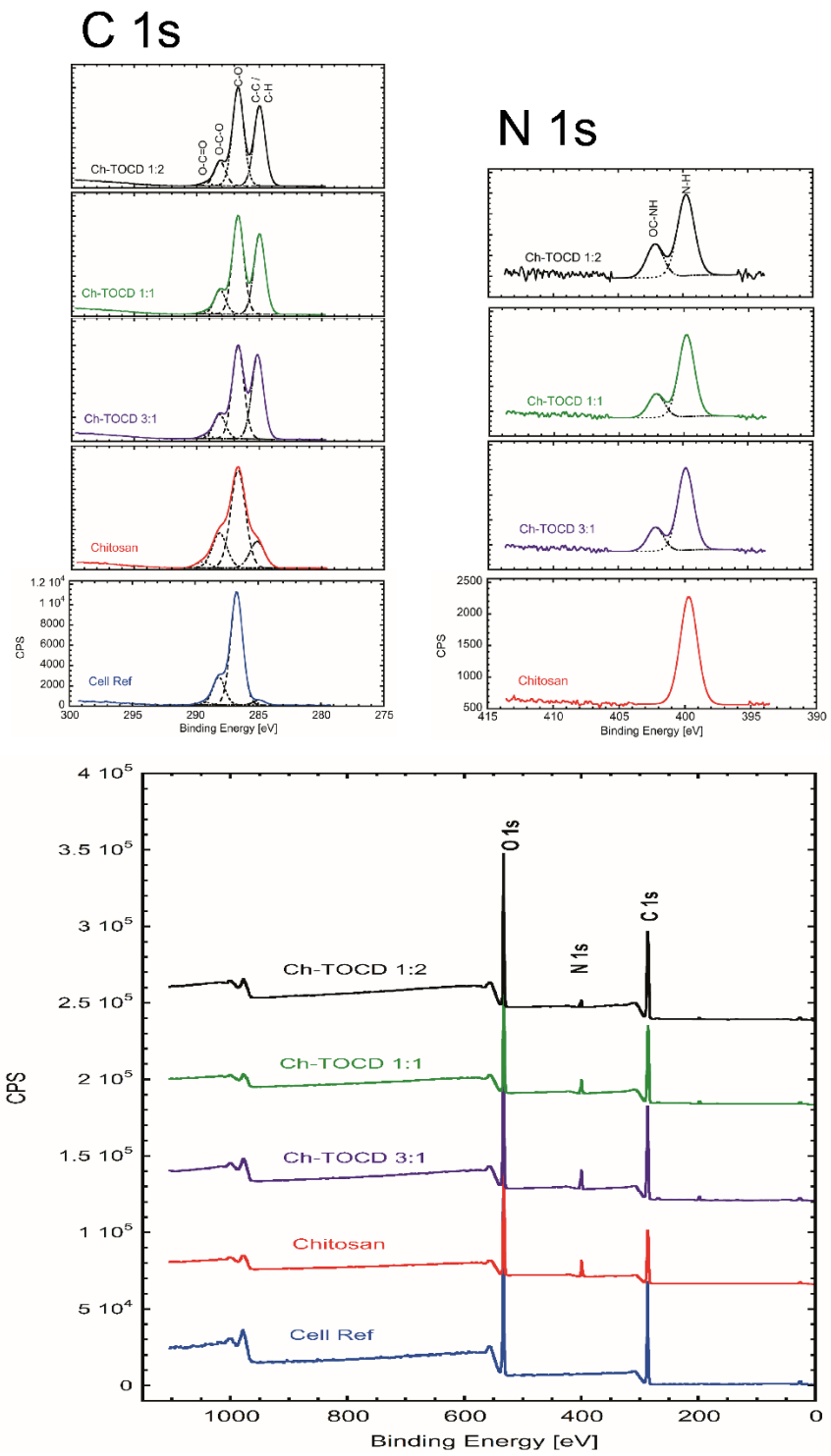

Figure 3. XPS wide energy region spectra of a reference cellulose, chitosan and the chitosan-TOCD conjugates. Above, the high-resolution C 1s (left) and N 1s (right) graphs are also presented.

Furthermore, FTIR spectra was obtained for all the different conjugates (Figure 4). It should be noted here that the carbonyl band at1740 cm^{-1} is clearly visible for the TOCD, whereas the conjugates do not possess such a band. This can be explained by the formation of the amide bonds between the carboxyl groups of TOCD and the amine groups of chitosan, which should reduce the carbonyl band originating from protonated carboxylic acid. Moreover, the NH bending band of derivatives was decreased while compared to that of the chitosan. This is likely due to the overlapping of the signal from the newly formed -CONH- linkages at the bands around 1645 to 1550 cm^{-1} [78]. Other changes can be seen in the bands related to the CH bonding, which may be explained by the presence of a high number of such bonds and the differences of the mobility between the polymer chains. Finally, it is worth mentioning that the band used to normalize the spectra was 1079 cm^{-1} for chitosan and all the derivatives, while for TOCD, C-O-C a band at 1027 cm^{-1} was used. However, the spectrum for Ch-TOCD 2:1 displayed nearly the same intensity in both bands, indicating a higher content of TOCD. The overlapping of the NH, OH-C=O, and HN-C=O between 1700-1500 cm^{-1}, also confirms a higher degree of modification in the Ch-TOCD 1:2.

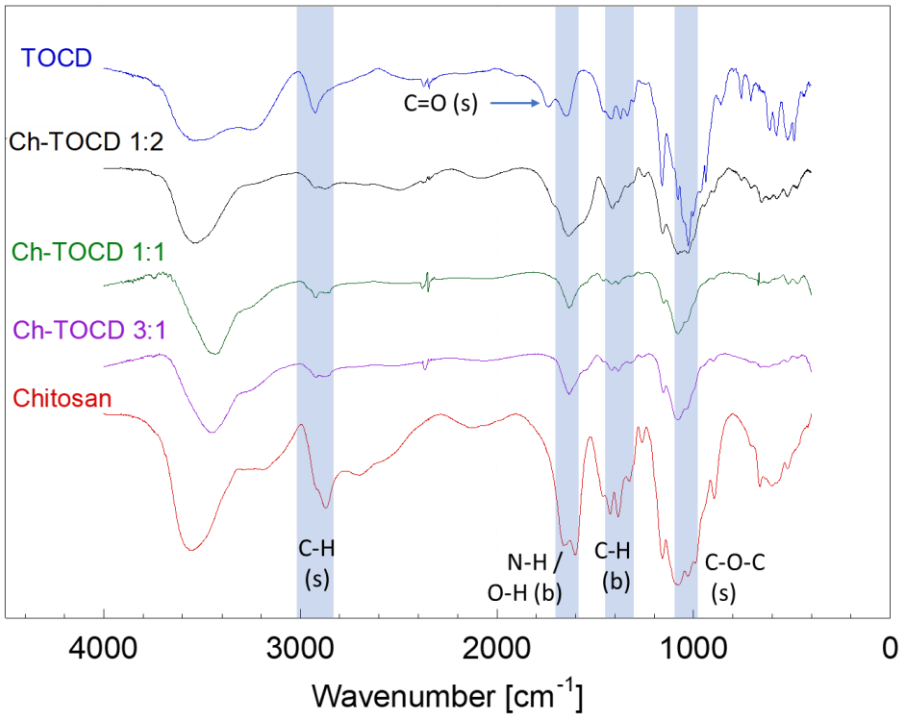

Figure 4. FTIR spectra comparison of the chitosan derivatives and the pristine materials.

3.3. Adsorption of Ch-TOCD onto CNF and microcystin-LR capture on the model surface.

The QCM-D sensograms for the formation of the CNF surface, the adsorption of the materials, and the capturing of microcystin-LR in saline conditions are shown in Figure 5. All sensograms have a reproducible frequency shift of – 5.08 and -124.50 Hz and dissipation shift of 1.15 and 43.17 ppm for the adsorption of both PEI and CNF.

The adsorption of the Ch and Ch-TOCDs onto the CNF surface in the 50 mM buffer medium revealed frequency shifts of -24.71 ± 0.04, -22.76 ± 0.07, -27.13 ± 0.05, and -35.56 ± 0.16 Hz for Ch, Ch-TOCD 1:2, Ch-TOCD 1:1, and Ch-TOCD 3:1, respectively. It is noteworthy that the total adsorbed mass does not seem to correlate with the DS value as the unmodified chitosan had adsorption level comparable to that of the chitosan-cyclodextrin DS 0.57.

While the MC-LR was introduced onto the aforementioned surfaces, a frequency decrease of ca. 5 Hz was observed for the Ch-TOCD 1:2, Ch-TOCD 1:1 and Ch-TOCD 3:1. The adsorption of MC-LR onto Ch surface resulted in a frequency decrease of 4 Hz. However, a buffer rinsing was found to release the mass from the surfaces as a decrease in dissipation and an increase in frequency were observed for all the systems. In fact, the final dissipation values of Ch, Ch-TOCD 1:1 and Ch-TOCD 3:1were found to be below the initial level of MC-LR adsorption. Conversely, the surface containing Ch-TOCD 2:1 also showed desorption, but with the final dissipation value remaining above the initial adsorption of MC-LR. Observed frequency and dissipation shifts can be attributed to the desorption of previously bound salts and water, rather than the interactions of polysaccharides with the MC-LR.

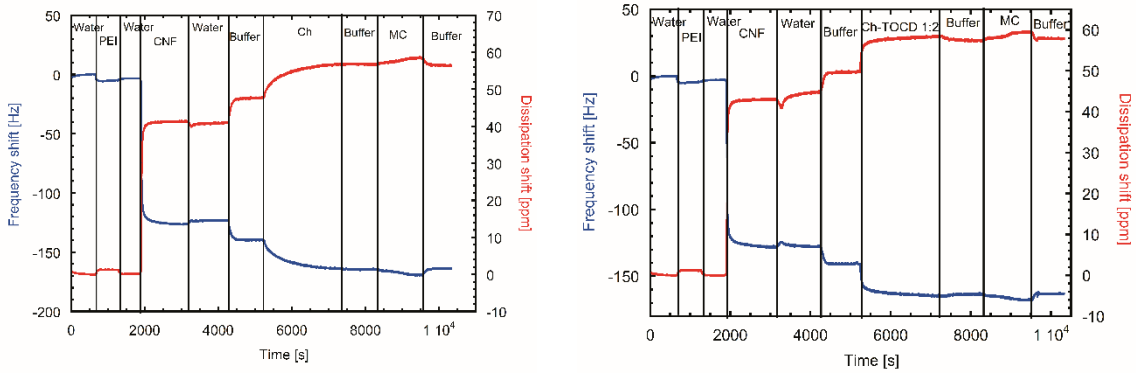

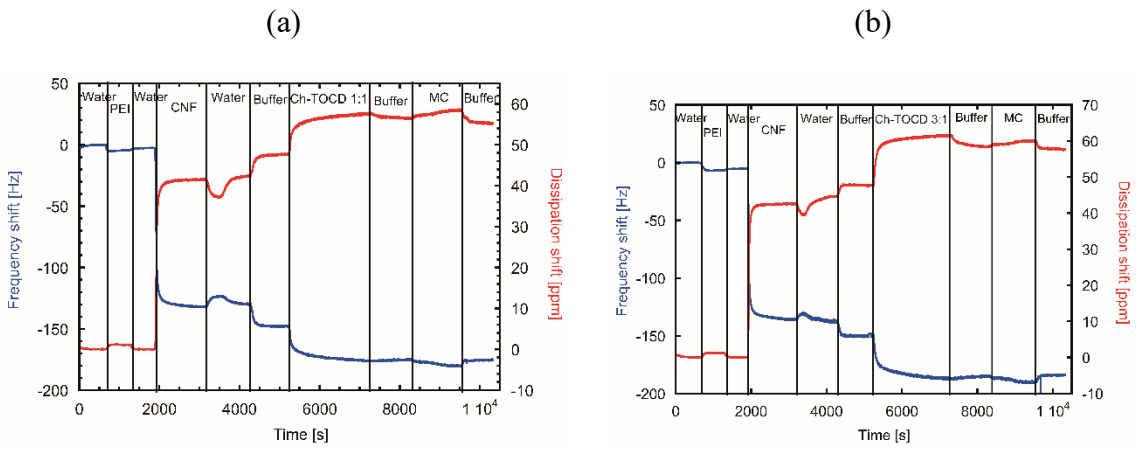

Figure 5. QCM-D sensograms of surface generation of CNF with chitosan and Ch-TOCD conjugates, followed by the adsorption of microcystin on 50 mM NaOAc buffer. Chitosan surface (a), Chitosan-TOCD molar ratio 1:2 (b), 1:1 (c), and 3:1 (d).

The corresponding adsorbed masses were calculated by fitting the QCM-D data into the BroadFit model and the obtained results are shown in Figure 6. It can be seen that the adsorbed masses of Chitosan, Ch-TOCD 1:1 and Ch-TOCD 3:1 onto the CNF surface are slightly higher than that of the Ch-TOCD 1:2. This may be partially explained by the number of unconjugated amino groups available for hydrogen bonding and electrostatic interaction with the CNF as well as by the different solubility of the Ch-TOCD conjugates in water, i.e., the larger presence of cyclodextrin (higher DS, Ch-TOCD 1:2) increased the water solubility of the conjugate, and therefore its adsorption to the surface is less favored [82]. However, the adsorption behavior of the rest of the polymers did not follow the correlation between the number of unconjugated amino groups and the electrostatic driven adsorption. These results indicate that the combined effect of H-bonding between β-(1 → 4) polysaccharides and the preferent entropic behavior - the exchange of bound water for the less soluble polymers – are the main driving mechanisms for the adsorption [83].

Positive MC-LR adsorption was only observed in the case of the surface coated with Ch-TOCD 1:2. However, as previously suggested, frequency values returned to the original ones before the MC adsorption while positive changes in dissipation were present after rinsing, which indicates swelling. This suggests that the changes observed in adsorbed mass are most

likely a tradeoff between toxin adsorption and loss of salts and release of water molecules. Adsorption capacity was estimated to be 20.5 mg/g for the Ch-TOCD 1:2 coated surface.

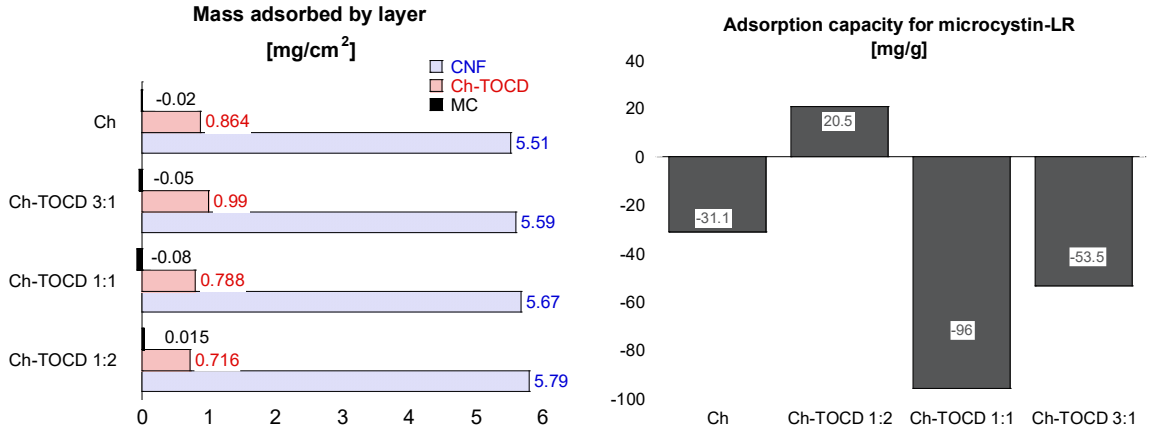

Figure 6. Mass adsorbed onto the PEI surface represented as layers of each individual component (left), and total adsorbed mass of microcystin on chitosan and Ch-TOCD surfaces (right).

3.4. Adsorption of Ch-TOCD onto CNF beads and microcystin-LR capture on 3-D environment.

MC-LR adsorption was also investigated by using a 3-D model comprising CNF beads which were produced by dissolving the lignocellulosic material in the sodium/urea solvent system followed by its regeneration in nitric acid media [84–86]. In this work, a mechanically produced bleached softwood nanocellulose was used as a starting material. It should be noted here that beads of similar size, shape, and structure as those produced by using dissolving pulp were obtained [87]. Figure S1a indicates the successful adsorption/coating of the TOCD-modified chitosan on the CNF beads as the solid content is increasing from a 2.6 ± 0.3% (uncoated CNF) to a maximum of 3.3 ± 0.2% (coated with the Ch-TOCD 1:2). The coating process was also monitored by the elemental analysis (Figure S2b). The carbon content decreased from 55% for the CNF beads to around 39% for the coated beads; however, the N% was between 0.12 and 0.15% for the different coated beads, showing no clear trend as the DS of the coating changed. Finally, FTIR spectra of the coated and uncoated systems were not conclusive regarding groups containing nitrogen, for coated and uncoated CNF. Contrary to what it was observed with the coated CNF, in the case of TOCD with higher

content of TOCD, a clear band of unmodified carboxyl groups was observed around 1750 $cm^{-1,}$ and the stretching of the freer C-H of the cyclodextrin around 2900 cm^{-1} (Figure S2c). Based on the previous results, the CNF beads coated with Ch-TOCD 1:2 was selected as a matrix to evaluate the MC-LR adsorption which was followed by HPLC analysis. As can be seen from the adsorption kinetics (Figure 7), the initial adsorption of MC-LR occurs faster with uncoated CNF beads (control) while compared to that of coated CNF beads. However, the final adsorbed amount of MC-LR was found to be slightly higher when coated CNF beads were used, i.e., after 24 h exposure to the MC-LR solution, the coated CNF beads were able to capture 2.4 mg/g of the pollutant while the capture with uncoated CNF beads reached 1.9 mg/g. It is worth mentioning here that these values are higher than those reported for cellulose surface regenerated by dissolving the cellulose in ionic liquids without chitosan, but lower than for the composite generated with 20% of chitosan which has an adsorption of around 20 mg/g [30].

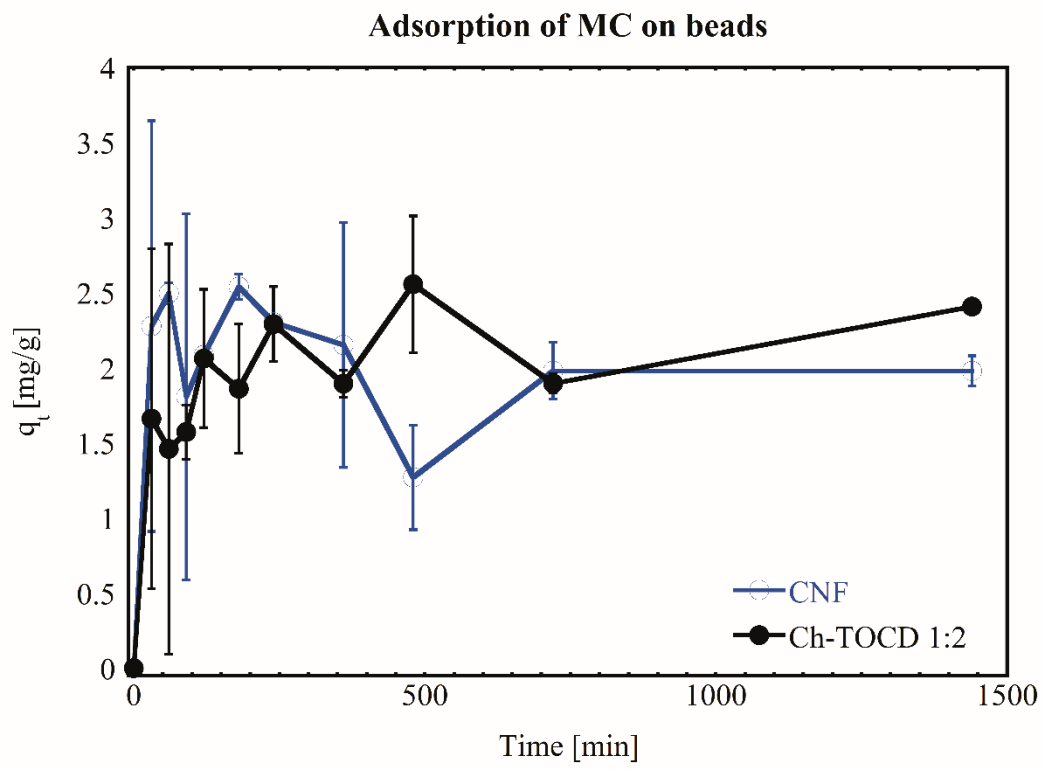

Figure 7. Adsorption kinetics of the CNF beads and CNF beads coated with Ch-TOCD 1:2 on a 6.5µg/mL solution of MC-LR over 24 h.

After fitting the adsorption data into pseudo-second order kinetic model (Figure 8), the equilibrium adsorption of MC-LR was 1.92 mg/g for the uncoated CNF beads and of 2.36 mg/g for the coated CNF beads with a R^2 of 0.96 and 0.98, respectively. When the k value was analyzed, the saturation half-time was found to be 7.97 min for the uncoated CNF beads and 81.3 min for the coated CNF beads. This significantly longer saturation half-time clearly indicates that the adsorption of MC-LR on the coated CNF beads rather follows the passive pathway than is driven by the cavity-substrate interactions and/or osmotic effects which are traditionally observed for cellulosic hydrogel-based adsorbents [83]. Furthermore, as only 0.7% of the mass of the coated bead corresponds to the coating -(Figure S2a), the slow kinetics can also be related to the hindered availability of active sites on the surface rather than the osmotic equilibrium of the concentration of MC-LR on the media and the bead.

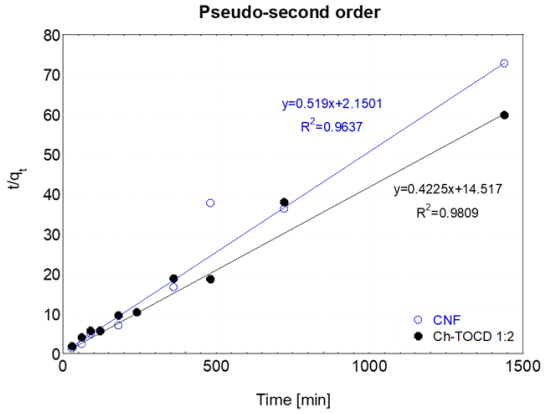

	CNF	Ch-TOCD 1:2
q_e	1.925	2.367
h	0.465	0.069
k_2	0.125	0.012
R^2	0.963	0.981
$t_{0.5}$	7.97	81.3

Figure 8. Pseudo-second order kinetic model for the uncoated CNF beads and CNF beads coated with Ch-TOCD 1:2.

These results show a successful coating of the CNF beads with the chitosan-cyclodextrin polymer, which had an active site that interacts with MC-LR through a different mechanism than the uncoated beads. However, the data obtained from the HPLC is ten-fold lower than the adsorption calculated from the 2D model (thin films) with QCM-D. This difference may be attributed to the differences in coverage and diffusion profiles of the CNF beads and thin films.

Presented methodology for the coating of the CNF beads with chitosan-cyclodextrin copolymer opens new venues for adding hydrophobic cavities on bio-based materials which

could be used for either capturing toxic aromatic molecules (e.g. chlorophenols) or for slow delivery of active ingredients (e.g. estradiol) in sutures or other fibers. [50,88,89].

4. Conclusions

In this work, a biopolymer-based concept for water purification was explored. Our approach comprises the modification of chitosan with TEMPO oxidized β-cyclodextrin and the subsequent adsorption of the synthesized conjugate (Ch-TOCD) onto cellulose surface, which was used as a platform to capture an amphipathic toxin (microcystin-LR). Three different conjugates were prepared by using EDC/NHS coupling chemistry with varied molar ratios of the functional groups (NH_2 and COOH) of the starting polymers. The adsorption of the conjugates on two distinct cellulose surfaces, namely cellulose nanofibrils (CNF) thin films and CNF beads, was monitored by Quartz Crystal Microbalance with Dissipation monitoring (QCM-D) and High-performance liquid chromatography (HPLC).

Finally, the coated nanocellulose-based materials were tested for their capacity to capture microcystin-LR. It was found that the CNF thin film coated with Ch-TOCD 1:2 was able to retain 20.5 mg/g whereas the CNF beads were able to capture only 2.36 mg/g. The difference in these values is most likely a consequence of an incomplete saturation of the coating on the beads. However, the difference in the kinetic modelling between the non-coated and coated CNF beads reflects a clear variation in adsorption mechanisms between the two materials. The successful adsorption of the coating on the lignocellulosic structure, as well as their capacity to adsorb an amphipathic molecule driven by its hydrophobic residue, airs that this bio-based coating has potential for a wide range of applications from drug delivery to water treatment.

Supplementary Information

Table S1 presents the XPS extracted data showing the position of each deconvoluted signal, the atomic content percentage of each bond, and the C/N ratio for the cellulose and chitosan references as well as the modified materials. Figure S1 presents the comparison between the spectra from β-cyclodextrin, and TEMPO mediated oxidized β-cyclodextrin. Figure S2 has the Physicochemical comparison of the uncoated cellulose beads coated with chitosan (Ch)

and chitosan-TOCD conjugates (Ch-TOCD 1:1, Ch-TOCD 1;2 and Ch-TOCD 3:1) by a) solid content: b) elemental analysis; and c) FTIR spectra.

CRediT authorship contribution statement

Diego Gomez-Maldonado: Conceptualization, Methodology, Investigation, Writing. **Ilari Filpponen:** Conceptualization, Methodology, Supervision, Writing. **Iris B. Vega Erramuspe:** Methodology, Investigation. **Leena-Sisko Johansson:** Investigation, Resources. **María Fernanda Mori:** Investigation, Writing. **Jayachandra Babu Ramapuram:** Methodology, Resources**. Matthew N. Waters:** Methodology, Resources. **Maria S. Peresin:** Conceptualization, Methodology, Supervision, Resources, Writing.

Conflicts of Interest

The authors declare no conflict of interest.

Acknowledgements

This work was supported by the National Science Foundation CAREER award 2119809 through the BMAT program in the Division of Materials Research and the EPSCoR program. Support was also provided by the USDA National Institute of Food and Agriculture, Hatch program (ALA013-17003) and McIntire-Stennis program (1022526). The School of Forestry and Wildlife Sciences at Auburn University's financial support to complete this work is much appreciated. This work made use of Aalto University Bioeconomy Facilities (the XPS statement), the FinnCERES – Competence Centre for the Materials Bioeconomy support is highly appreciated.

References

[1] E. Shim, Smart surface treatments for textiles for protection, in: Smart Text. Prot., Elsevier, 2013: pp. 87–126. https://doi.org/10.1533/9780857097620.1.87.

[2] S. Solgi, R. Ghorbani-Vaghei, S. Alavinia, Application of copper iodide nanoparticles immobolized porous polysulfonamide gel as an effective nanocatalyst for synthesis of aminoindolizines, J. Porous Mater. (2020). https://doi.org/10.1007/s10934-020-00989-8.

[3] J. Guo, I. Filpponen, P. Su, J. Laine, O.J. Rojas, Attachment of gold nanoparticles on cellulose nanofibrils via click reactions and electrostatic interactions, Cellulose. 23 (2016) 3065–3075. https://doi.org/10.1007/s10570-016-1042-7.

[4] P.K. Huang, J.W. Yeh, T.T. Shun, S.K. Chen, Multi-principal-element alloys with improved oxidation and wear resistance for thermal spray coating, Adv. Eng. Mater. 6 (2004) 74–78. https://doi.org/10.1002/adem.200300507.

[5] M. Parvinzadeh, F. Alimohammadi, A. Shamei, Surface & Coatings Technology Preparation of water-repellent cellulose fi bers using a polycarboxylic acid / hydrophobic silica nanocomposite coating, Surf.

Coat. Technol. 206 (2012) 3208–3215. https://doi.org/10.1016/j.surfcoat.2012.01.006.

[6] T.T. Isimjan, T. Wang, S. Rohani, A novel method to prepare superhydrophobic, UV resistance and anti-corrosion steel surface, Chem. Eng. J. 210 (2012) 182–187. https://doi.org/10.1016/j.cej.2012.08.090.

[7] E. Larsson, C.C. Sanchez, C. Porsch, E. Karabulut, L. Wågberg, A. Carlmark, Thermo-responsive nanofibrillated cellulose by polyelectrolyte adsorption, Eur. Polym. J. 49 (2013) 2689–2696. https://doi.org/10.1016/j.eurpolymj.2013.05.023.

[8] M. Zhang, W. Ma, J. Cui, S. Wu, J. Han, Y. Zou, C. Huang, Hydrothermal synthesized UV-resistance and transparent coating composited superoloephilic electrospun membrane for high efficiency oily wastewater treatment, J. Hazard. Mater. 383 (2020) 121152. https://doi.org/10.1016/j.jhazmat.2019.121152.

[9] F. Kayaci, Z. Aytac, T. Uyar, Surface modification of electrospun polyester nanofibers with cyclodextrin polymer for the removal of phenanthrene from aqueous solution, J. Hazard. Mater. 261 (2013) 286–294. https://doi.org/10.1016/j.jhazmat.2013.07.041.

[10] Z. Karim, S. Claudpierre, M. Grahn, K. Oksman, A.P. Mathew, Nanocellulose based functional membranes for water cleaning: Tailoring of mechanical properties, porosity and metal ion capture, J. Memb. Sci. 514 (2016) 418–428. https://doi.org/10.1016/j.memsci.2016.05.018.

[11] R.H. Fang, A. V. Kroll, W. Gao, L. Zhang, Cell Membrane Coating Nanotechnology, Adv. Mater. 30 (2018) 1–34. https://doi.org/10.1002/adma.201706759.

[12] J. Groll, J. Fiedler, E. Engelhard, T. Ameringer, S. Tugulu, H.A. Klok, R.E. Brenner, M. Moeller, A novel star PEG-derived surface coating for specific cell adhesion, J. Biomed. Mater. Res. - Part A. 74 (2005) 607–617. https://doi.org/10.1002/jbm.a.30335.

[13] I. Ali, New generation adsorbents for water treatment, Chem. Rev. 112 (2012) 5073–5091. https://doi.org/10.1021/cr300133d.

[14] W.J. Huang, B.L. Cheng, Y.L. Cheng, Adsorption of microcystin-LR by three types of activated carbon, J. Hazard. Mater. 141 (2007) 115–122. https://doi.org/10.1016/j.jhazmat.2006.06.122.

[15] D. Gomez-Maldonado, I.B. Vega Erramuspe, I. Filpponen, L.-S. Johansson, S. Lombardo, J. Zhu, W. Thielemans, M.S. Peresin, Cellulose-Cyclodextrin Co-Polymer for the Removal of Cyanotoxins on Water Sources, Polymers (Basel). 11 (2019) 2075. https://doi.org/10.3390/polym11122075.

[16] K.L. Spence, R.A. Venditti, O.J. Rojas, Y. Habibi, J.J. Pawlak, The effect of chemical composition on microfibrillar cellulose films from wood pulps: Water interactions and physical properties for packaging applications, Cellulose. 17 (2010) 835–848. https://doi.org/10.1007/s10570-010-9424-8.

[17] M.S. Peresin, A.H. Vesterinen, Y. Habibi, L.S. Johansson, J.J. Pawlak, A.A. Nevzorov, O.J. Rojas, Crosslinked PVA nanofibers reinforced with cellulose nanocrystals: Water interactions and thermomechanical properties, J. Appl. Polym. Sci. 131 (2014) 1–12. https://doi.org/10.1002/app.40334.

[18] D. Zeng, J. Wu, J.F. Kennedy, Application of a chitosan flocculant to water treatment, Carbohydr. Polym. 71 (2008) 135–139. https://doi.org/10.1016/j.carbpol.2007.07.039.

[19] J. Trygg, E. Yildir, R. Kolakovic, N. Sandler, P. Fardim, Anionic cellulose beads for drug encapsulation

and release, Cellulose. 21 (2014) 1945–1955. https://doi.org/10.1007/s10570-014-0253-z.

[20] M.O. Adebajo, R.L. Frost, J.T. Kloprogge, O. Carmody, S. Kokot, Porous Materials for Oil Spill Cleanup: A Review of Synthesis and Absorbing Properties, J. Porous Mater. 10 (2003) 159–170. https://doi.org/10.1023/A:1027484117065.

[21] B. Arkles, Hydrophobicity, Hydrophilicity and Silanes, Paint Coatings Ind. (2006) 114. https://doi.org/10.1016/j.micromeso.2005.05.031.

[22] T. Mishima, M. Hisamatsu, W.S. York, K. Teranishi, T. Yamada, Adhesion of β-D-glucans to cellulose, Carbohydr. Res. 308 (1998) 389–395. https://doi.org/10.1016/S0008-6215(98)00099-8.

[23] K. Junka, I. Filpponen, L.S. Johansson, E. Kontturi, O.J. Rojas, J. Laine, A method for the heterogeneous modification of nanofibrillar cellulose in aqueous media, Carbohydr. Polym. 100 (2014) 107–115. https://doi.org/10.1016/j.carbpol.2012.11.063.

[24] A. Dufresne, Nanocellulose: From nature to high performance tailored materials, 2nd ed., De Gruyter, Germany, 2017.

[25] J.W.C. Dunlop, P. Fratzl, Biological Composites, Annu. Rev. Mater. Res. 40 (2010) 1–24. https://doi.org/10.1146/annurev-matsci-070909-104421.

[26] K. Pillai, F. Navarro Arzate, W. Zhang, S. Renneckar, Towards Biomimicking Wood: Fabricated Free-standing Films of Nanocellulose, Lignin, and a Synthetic Polycation, J. Vis. Exp. (2014) 1–14. https://doi.org/10.3791/51257.

[27] H. Dong, J.F. Snyder, D.T. Tran, J.L. Leadore, Hydrogel, aerogel and film of cellulose nanofibrils functionalized with silver nanoparticles, Carbohydr. Polym. 95 (2013) 760–767. https://doi.org/10.1016/j.carbpol.2013.03.041.

[28] P. Kumar Dutta, J. Dutta, V.S. Tripathi, Chitin and chitosan: Chemistry, properties and applications, J. Sci. Ind. Res. 63 (2004) 20–31. https://doi.org/10.1002/chin.200727270.

[29] R.S. Blackburn, Natural polysaccharides and their interactions with dye molecules: Applications in effluent treatment, Environ. Sci. Technol. 38 (2004) 4905–4909. https://doi.org/10.1021/es049972n.

[30] C.D. Tran, S. Duri, A. Delneri, M. Franko, Chitosan-cellulose composite materials : Preparation , Characterization and application for removal of microcystin, J. Hazard. Mater. 253 (2013) 355–366.

[31] H. Sashiwa, Y. Shigemasa, R. Roy, Dissolution of Chitosan in Dimethyl Sulfoxide by Salt Formation, Chem. Lett. 29 (2004) 596–597. https://doi.org/10.1246/cl.2000.596.

[32] P. Mocchiutti, C.N. Schnell, G.D. Rossi, M.S. Peresin, M.A. Zanuttini, M. V. Galván, Cationic and anionic polyelectrolyte complexes of xylan and chitosan. Interaction with lignocellulosic surfaces, Carbohydr. Polym. 150 (2016) 89–98. https://doi.org/10.1016/j.carbpol.2016.04.111.

[33] W. Saenger, T. Steiner, Cyclodextrin Inclusion Complexes: Host–Guest Interactions and Hydrogen-Bonding Networks, Acta Crystallogr. Sect. A Found. Crystallogr. 54 (1998) 798–805. https://doi.org/10.1107/S0108767398010733.

[34] A. Sinha, N.R. Jana, Separation of microcystin-LR by cyclodextrin-functionalized magnetic composite of colloidal graphene and porous silica, ACS Appl. Mater. Interfaces. 7 (2015) 9911–9919. https://doi.org/10.1021/acsami.5b02038.

[35] D. Gomez-Maldonado, A.M. Reynolds, L.-S. Johansson, D.J. Burnett, J.B. Ramapuram, M.N. Waters, I.B. Vega Erramuspe, M.S. Peresin, Fabrication of aerogels from cellulose nanofibril grafted with β-cyclodextrin for capture of water pollutants, J. Porous Mater. 28 (2021) 1725–1736. https://doi.org/10.1007/s10934-021-01109-w.

[36] D. Gomez-maldonado, A.M. Reynolds, L. Johansson, D.J. Burnett, J. Babu, M. Waters, I.B.V. Erramuspe, M.S. Peresin, Fabrication of aerogels from cellulose nanofibril grafted with β -cyclodextrin for capture of water pollutants . Keywords, (n.d.) 1–17.

[37] S. Kim, Y.S. Yun, Y.E. Choi, Development of waste biomass based sorbent for removal of cyanotoxin microcystin-LR from aqueous phases, Bioresour. Technol. 247 (2018) 690–696. https://doi.org/10.1016/j.biortech.2017.09.164.

[38] G. Yuan, M. Prabakaran, S. Qilong, J.S. Lee, I.M. Chung, M. Gopiraman, K.H. Song, I.S. Kim, Cyclodextrin functionalized cellulose nanofiber composites for the faster adsorption of toluene from aqueous solution, J. Taiwan Inst. Chem. Eng. 70 (2017) 352–358. https://doi.org/10.1016/j.jtice.2016.10.028.

[39] Y. Jiang, B. Liu, J. Xu, K. Pan, H. Hou, J. Hu, J. Yang, Cross-linked chitosan/β-cyclodextrin composite for selective removal of methyl orange: Adsorption performance and mechanism, Carbohydr. Polym. 182 (2018) 106–114. https://doi.org/10.1016/j.carbpol.2017.10.097.

[40] A.Z.M. Badruddoza, Z.B.Z. Shawon, W.J.D. Tay, K. Hidajat, M.S. Uddin, Fe 3O 4/cyclodextrin polymer nanocomposites for selective heavy metals removal from industrial wastewater, Carbohydr. Polym. 91 (2013) 322–332. https://doi.org/10.1016/j.carbpol.2012.08.030.

[41] D. Shao, G. Sheng, C. Chen, X. Wang, M. Nagatsu, Removal of polychlorinated biphenyls from aqueous solutions using β-cyclodextrin grafted multiwalled carbon nanotubes, Chemosphere. 79 (2010) 679–685. https://doi.org/10.1016/j.chemosphere.2010.03.008.

[42] P. Chen, H.W. Liang, X.H. Lv, H.Z. Zhu, H. Bin Yao, S.H. Yu, Carbonaceous nanofiber membrane functionalized by beta-cyclodextrins for molecular filtration, ACS Nano. 5 (2011) 5928–5935. https://doi.org/10.1021/nn201719g.

[43] S. Khaoulani, H. Chaker, C. Cadet, E. Bychkov, L. Cherif, A. Benguedach, S. Fourmentin, Wastewater treatment by cyclodextrin polymers and noble metal/mesoporous TiO2photocatalysts, Comptes Rendus Chim. 18 (2015) 23–31. https://doi.org/10.1016/j.crci.2014.07.004.

[44] H. Liu, X. Cai, Y. Wang, J. Chen, Adsorption mechanism-based screening of cyclodextrin polymers for adsorption and separation of pesticides from water, Water Res. 45 (2011) 3499–3511. https://doi.org/10.1016/j.watres.2011.04.004.

[45] H. Kono, K. Onishi, T. Nakamura, Characterization and bisphenol A adsorption capacity of β-cyclodextrin-carboxymethylcellulose-based hydrogels, Carbohydr. Polym. 98 (2013) 784–792. https://doi.org/10.1016/j.carbpol.2013.06.065.

[46] A.R. Khan, P. Forgo, K.J. Stine, V.T. D'Souza, Methods for selective modifications of cyclodextrins, Chem. Rev. 98 (1998) 1977–1996. https://doi.org/10.1021/cr970012b.

[47] C.F. Huang, C.W. Tu, R.H. Lee, C.H. Yang, W.C. Hung, K.Y. Andrew Lin, Study of various diameter

716 and functionality of TEMPO-oxidized cellulose nanofibers on paraquat adsorptions, Polym. Degrad.
717 Stab. 161 (2019) 206–212. https://doi.org/10.1016/j.polymdegradstab.2019.01.023.
718 [48] C.F. Huang, J.K. Chen, T.Y. Tsai, Y.A. Hsieh, K.Y. Andrew Lin, Dual-functionalized cellulose
719 nanofibrils prepared through TEMPO-mediated oxidation and surface-initiated ATRP, Polymer
720 (Guildf). 72 (2015) 395–405. https://doi.org/10.1016/j.polymer.2015.02.056.
721 [49] T. Saito, A. Isogai, TEMPO-mediated oxidation of native cellulose. The effect of oxidation conditions
722 on chemical and crystal structures of the water-insoluble fractions, Biomacromolecules. 5 (2004) 1983–
723 1989. https://doi.org/10.1021/bm0497769.
724 [50] H. Orelma, T. Virtanen, S. Spoljaric, J. Lehmonen, J. Seppälä, O.J. Rojas, A. Harlin, Cyclodextrin-
725 Functionalized Fiber Yarns Spun from Deep Eutectic Cellulose Solutions for Nonspecific Hormone
726 Capture in Aqueous Matrices, Biomacromolecules. 19 (2018) 652–661.
727 https://doi.org/10.1021/acs.biomac.7b01765.
728 [51] M. Prabaharan, S. Gong, Novel thiolated carboxymethyl chitosan-g-β-cyclodextrin as mucoadhesive
729 hydrophobic drug delivery carriers, Carbohydr. Polym. 73 (2008) 117–125.
730 https://doi.org/10.1016/j.carbpol.2007.11.005.
731 [52] H. Orelma, I. Filpponen, L.S. Johansson, M. Österberg, O.J. Rojas, J. Laine, Surface functionalized
732 nanofibrillar cellulose (NFC) film as a platform for immunoassays and diagnostics, Biointerphases. 7
733 (2012) 1–12. https://doi.org/10.1007/s13758-012-0061-7.
734 [53] M. D'Este, D. Eglin, M. Alini, A systematic analysis of DMTMM vs EDC/NHS for ligation of amines
735 to Hyaluronan in water, Carbohydr. Polym. 108 (2014) 239–246.
736 https://doi.org/10.1016/j.carbpol.2014.02.070.
737 [54] L. Li, L. Fan, M. Sun, H. Qiu, X. Li, H. Duan, C. Luo, Adsorbent for hydroquinone removal based on
738 graphene oxide functionalized with magnetic cyclodextrin-chitosan, Int. J. Biol. Macromol. 58 (2013)
739 169–175. https://doi.org/10.1016/j.ijbiomac.2013.03.058.
740 [55] T. Li, P. Huang, J. Liang, W. Fu, Z. Guo, L. Xu, Microcystin-LR (MCLR) Induces a Compensation
741 of PP2A Activity Mediated by α 4 Protein in HEK293 Cells, (2011).
742 [56] K.A. Loftin, J.M. Clark, C.A. Journey, D.W. Kolpin, P.C. Van Metre, D. Carlisle, P.M. Bradley, Spatial
743 and temporal variation in microcystin occurrence in wadeable streams in the southeastern United States,
744 Environ. Toxicol. Chem. 35 (2016) 2281–2287. https://doi.org/10.1002/etc.3391.
745 [57] Word Health Organization (WHO), Cyanobacterial toxins: Microcystin-LR in Drinking-water, Guidel.
746 Drink. Qual. 2 (1998).
747 [58] S. Merel, M.C. Villarín, K. Chung, S. Snyder, Spatial and thematic distribution of research on
748 cyanotoxins, Toxicon. 76 (2013) 118–131. https://doi.org/10.1016/j.toxicon.2013.09.008.
749 [59] R. Al-Ammar, A. Nabok, A. Hashim, T. Smith, Microcystin-LR produced by bacterial algae: Optical
750 detection and purification of contaminated substances, Sensors Actuators, B Chem. 209 (2015) 1070–
751 1076. https://doi.org/10.1016/j.snb.2014.11.063.
752 [60] J. Meriluoto, G.A. Codd, Cyanobacterial Monitoring and Cyanotoxin Analysis, 2005.
753 https://doi.org/10.1002/9781119068761.

[61] A.S. Archimandritis, T. Papadimitriou, K.A. Kormas, C.S. Laspidou, K. Yannakopoulou, Y.G. Lazarou, Theoretical investigation of microcystin-LR, microcystin-RR and nodularin-R complexation with α-, β-, and γ-cyclodextrin as a starting point for the targeted design of efficient cyanotoxin traps, Sustain. Chem. Pharm. 3 (2016) 25–32. https://doi.org/10.1016/j.scp.2016.02.001.

[62] T. Saito, M. Hirota, N. Tamura, S. Kimura, H. Fukuzumi, L. Heux, A. Isogai, Individualization of Nano-Sized Plant Cellulose Fibrils by Direct Surface Carboxylation Using TEMPO Catalyst under Neutral Conditions, Biomacromolecules. 10 (2009) 1992–1996. https://doi.org/10.1021/bm900414t.

[63] D. da Silva Perez, S. Montanari, M.R. Vignon, TEMPO-mediated oxidation of cellulose III, Biomacromolecules. 4 (2003) 1417–1425. https://doi.org/10.1021/bm034144s.

[64] P.J. Larkin, "IR and Raman Spectroscopy - Principles and Spectral Interpretation," 2011. https://doi.org/10.1016/b978-0-12-386984-5.10001-1.

[65] L. Johansson, J.M. Campbell, O.J. Rojas, Cellulose as the in situ reference for organic XPS. Why? Because it works, Surf. Interface Anal. 52 (2020) 1134–1138. https://doi.org/10.1002/sia.6759.

[66] L.S. Johansson, J.M. Campbell, Reproducible XPS on biopolymers: Cellulose studies, Surf. Interface Anal. 36 (2004) 1018–1022. https://doi.org/10.1002/sia.1827.

[67] G. Beamson, D. Briggs, High resolution XPS of organic polymers: The Scienta ESCA 300 database, John Wiley & Sons, Chichester, 1992.

[68] N. Fairley, V. Fernandez, M. Richard-Plouet, C. Guillot-Deudon, J. Walton, E. Smith, D. Flahaut, M. Greiner, M. Biesinger, S. Tougaard, D. Morgan, J. Baltrusaitis, Systematic and collaborative approach to problem solving using X-ray photoelectron spectroscopy, (2021). https://doi.org/10.1016/j.apsadv.2021.100112.

[69] KSV Instruments Ltd, What Is a Quartz Crystal Microbalance – Qcm, (2002) 1–10.

[70] M. V. Voinova, M. Jonson, B. Kasemo, "Missing mass" effect in biosensor's QCM applications, Biosens. Bioelectron. 17 (2002) 835–841. https://doi.org/10.1016/S0956-5663(02)00050-7.

[71] A. Example, Dissipative QCM, Langmuir. (1991) 1–3.

[72] G. Sauerbrey, Verwendung von Schwingquarzen zur Wägung dünner Schichten und zur Mikrowägung, Zeitschrift Für Phys. 155 (1959) 206–222. https://doi.org/10.1007/BF01337937.

[73] M. V. Voinova, M. Rodahl, M. Jonson, B. Kasemo, Viscoelastic acoustic response of layered polymer films at fluid-solid interfaces: Continuum mechanics approach, (1998) 1–22. https://doi.org/10.1238/Physica.Regular.059a00391.

[74] X. Turon, O.J. Rojas, R.S. Deinhammer, Enzymatic kinetics of cellulose hydrolysis: A QCM-D study, Langmuir. 24 (2008) 3880–3887. https://doi.org/10.1021/la7032753.

[75] H. JIANG, Z. YANG, X. ZHOU, Y. FANG, H. JI, Immobilization of β-Cyclodextrin as Insoluble β-Cyclodextrin Polymer and Its Catalytic Performance, Chinese J. Chem. Eng. 20 (2012) 784–792. https://doi.org/10.1016/S1004-9541(11)60249-8.

[76] T. Saito, I. Shibata, A. Isogai, N. Suguri, N. Sumikawa, Distribution of carboxylate groups introduced into cotton linters by the TEMPO-mediated oxidation, Carbohydr. Polym. 61 (2005) 414–419. https://doi.org/10.1016/j.carbpol.2005.05.014.

[77] Y. Habibi, H. Chanzy, M.R. Vignon, TEMPO-mediated surface oxidation of cellulose whiskers, Cellulose. 13 (2006) 679–687. https://doi.org/10.1007/s10570-006-9075-y.

[78] C. Lai, S. Zhang, X. Chen, L. Sheng, Nanocomposite films based on TEMPO-mediated oxidized bacterial cellulose and chitosan, Cellulose. 21 (2014) 2757–2772. https://doi.org/10.1007/s10570-014-0330-3.

[79] P.C. Li, G.M. Liao, S.R. Kumar, C.M. Shih, C.C. Yang, D.M. Wang, S.J. Lue, Fabrication and Characterization of Chitosan Nanoparticle-Incorporated Quaternized Poly(Vinyl Alcohol) Composite Membranes as Solid Electrolytes for Direct Methanol Alkaline Fuel Cells, Electrochim. Acta. 187 (2016) 616–628. https://doi.org/10.1016/j.electacta.2015.11.117.

[80] G. Lawrie, I. Keen, B. Drew, A. Chandler-temple, L. Rintoul, P. Fredericks, L. Grøndahl, Interactions between Alginate and Chitosan Biopolymers Characterized Using FTIR and XPS, (2007) 2533–2541.

[81] A.M. Ferraria, S. Boufi, N. Battaglini, A.M.B. Do Rego, M. Reivilar, Hybrid systems of silver nanoparticles generated on cellulose surfaces, Langmuir. 26 (2010) 1996–2001. https://doi.org/10.1021/la902477q.

[82] T. Ristić, T. Mohan, R. Kargl, S. Hribernik, A. Doliška, K. Stana-Kleinschek, L. Fras, A study on the interaction of cationized chitosan with cellulose surfaces, Cellulose. 21 (2014) 2315–2325. https://doi.org/10.1007/s10570-014-0267-6.

[83] S. Lombardo, W. Thielemans, Thermodynamics of adsorption on nanocellulose surfaces, Cellulose. 26 (2019) 249–279. https://doi.org/10.1007/s10570-018-02239-2.

[84] J.J.J. O'Neill, E.P. Reichardt, Method of producing cellulose pellets, 2543928, 1951.

[85] P. Trivedi, T. Saloranta-Simell, U. Maver, L. Gradišnik, N. Prabhakar, J.-H. Smått, T. Mohan, M. Gericke, T. Heinze, P. Fardim, Chitosan–Cellulose Multifunctional Hydrogel Beads: Design, Characterization and Evaluation of Cytocompatibility with Breast Adenocarcinoma and Osteoblast Cells, Bioengineering. 5 (2018) 3. https://doi.org/10.3390/bioengineering5010003.

[86] J. Trygg, P. Fardim, M. Gericke, E. Mäkilä, J. Salonen, Physicochemical design of the morphology and ultrastructure of cellulose beads, Carbohydr. Polym. 93 (2013) 291–299. https://doi.org/10.1016/j.carbpol.2012.03.085.

[87] D. Gomez-Maldonado, I. Filpponen, J.A. Hernandez-Díaz, M.N. Waters, M.L. Auad, L.-S. Johansson, I.B. Vega-Erramuspe, M.S. Peresin, Simple functionalization of cellulose beads with pre-propargylated chitosan for clickable scaffold substrates, Cellulose. 28 (2021) 6073–6087. https://doi.org/10.1007/s10570-021-03905-8.

[88] F. Zhang, W. Wu, S. Sharma, G. Tong, Y. Deng, Synthesis of Cyclodextrin-functionalized Cellulose Nanofibril Aerogel as a Highly Effective Adsorbent for Phenol Pollutant Removal, BioResources. 10 (2015) 7555–7568.

[89] M.H. Mohamed, L.D. Wilson, J. V. Headley, K.M. Peru, Investigation of the sorption properties of β-cyclodextrin-based polyurethanes with phenolic dyes and naphthenates, J. Colloid Interface Sci. 356 (2011) 217–226. https://doi.org/10.1016/j.jcis.2010.11.002.

829
830

Supplementary Information

Development of a β-cyclodextrin-chitosan polymer as active coating for cellulosic surfaces and capturing of microcystin-LR

Diego Gomez-Maldonado [a], Ilari Filpponen [b], Iris B. Vega Erramuspe [a], Leena-Sisko Johansson [c], María Fernanda Mori [d], Ramapuram Jayachandra Babu [e], Matthew N. Waters [f], Maria S. Peresin [a] *

[a] Forest Products Development Center; College of Forestry, Wildlife and Environment, Auburn University. 602 Duncan Drive, 36849, Auburn. Alabama, USA
[b] Department of Chemical Engineering, Alabama Center for Paper and Bioresource Engineering (AC-PABE), Auburn University, Auburn, Alabama 36849, USA
[c] Department of Bioprocesses and Biosystems, School of Chemical Engineering, Aalto University, Aalto FI-00076, Finland
[d] Instituto de Investigaciones en Catálisis y Petroquímica, CONICET, Facultad de Ingeniería Química, Universidad Nacional del Litoral, Santiago del Estero 2829, S3000AOM Santa Fe, Argentina
[e] Harrison School of Pharmacy, Auburn University, Auburn, AL 36849, United States
[f] Department of Crop, Soil and Environmental Sciences, Auburn University, Auburn, Alabama 36849, USA

Table S1. XPS extracted data showing the position of each deconvoluted signal, the atomic content percentage of each bond, and the C/N ratio for the cellulose and chitosan references as well as the modified materials.

			Atomic Concentration (%)				
		position (eV)	Cellulose reference	Chitosan	Ch-TOCD 3:1	Ch-TOCD 1:1	Ch-TOCD 1:2
C 1s	C-H/ -C-C	285.0 ± 0.2	1.9	9.1	8.4	28.0	26.5
	C-O	286.7	44.0	33.4	39.7	31.0	32.5
	O-C-O	288.0 ± 0.2	10.8	11.9	9.6	8.1	8.0
	O-C=O	289.3 ± 0.2	1.0	2.0	0.8	1.0	0.9
N 1s	N-H	399.8 ± 0.1	N/A	7.7	5.5	4.8	2.1
	OC-NH	402.1 ± 0.1	N/A	-	1.6	1.4	0.9
O 1s		533.2	42.7	32.3	34.4	25.7	29.2
	Ratio C/N		N/A	7.8	8.2	10.9	22.9

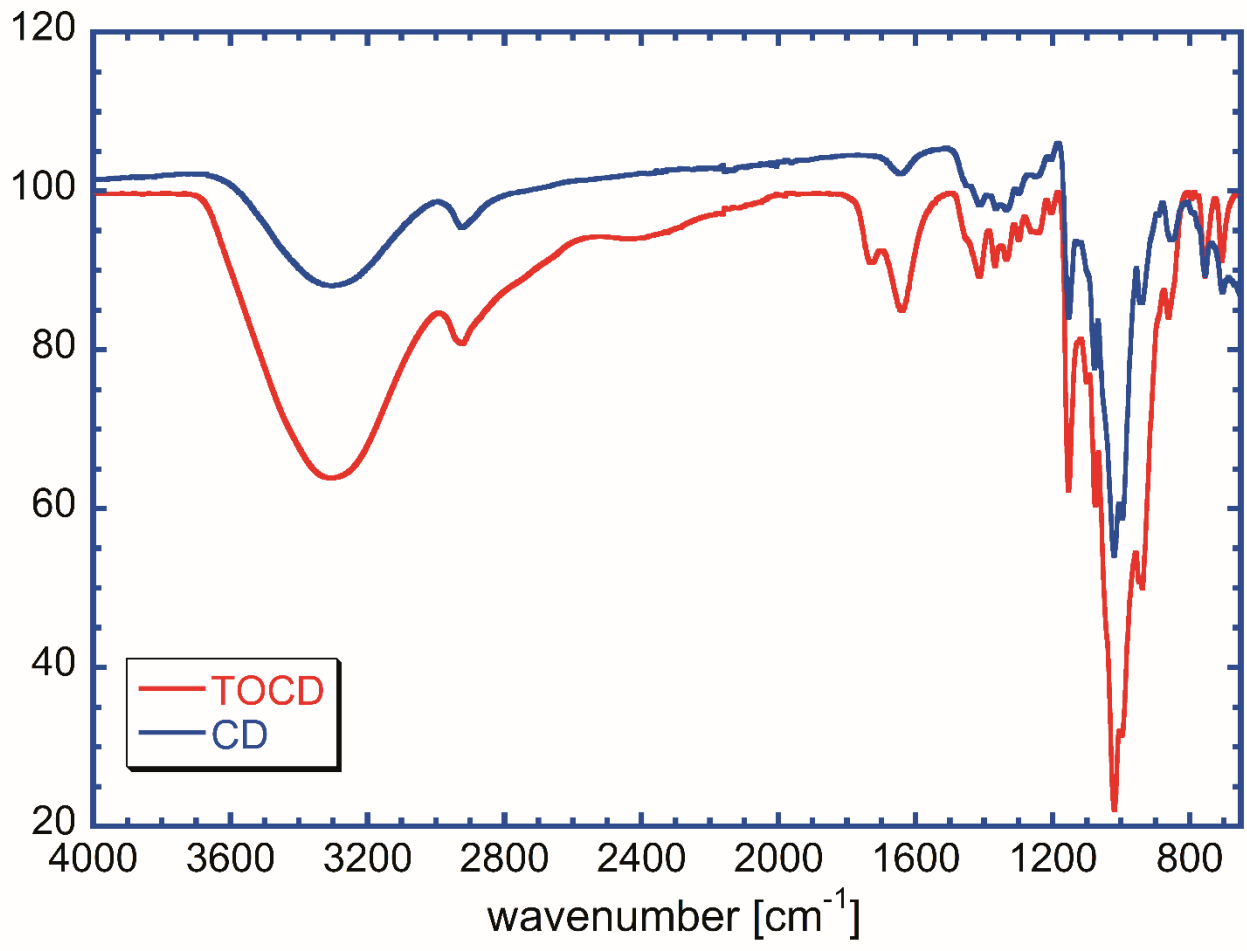

Figure S1. FTIR-ATR spectra of the unmodified β-cyclodextrin (CD) and the TEMPO mediated oxidized cyclodextrin (TOCD).

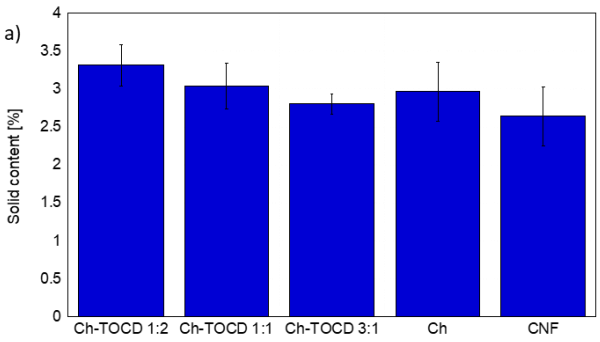

b)

	%C	%N	C/N
CNF	54.98	N/A	N/A
Chitosan	40.28	0.15	268.5
Ch-TOCD 1:2 (NH: COOH)	39.55	0.13	304.2
Ch-TOCD 1:1 (NH: COOH)	39.33	0.14	280.9
Ch-TOCD 3:1 (NH: COOH)	39.80	0.12	331.7

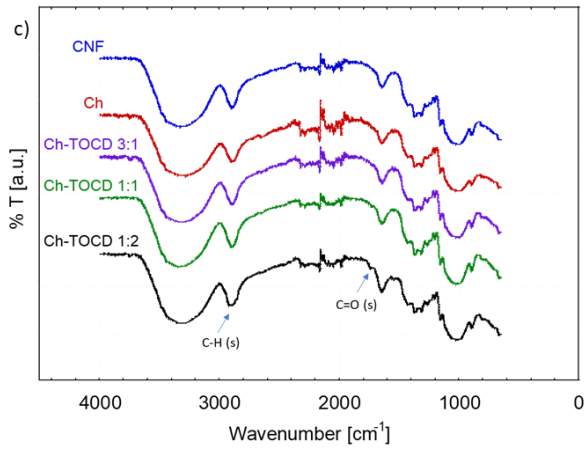

Figure S2. Physicochemical comparison of the uncoated cellulose beads coated with chitosan (Ch) and chitosan-TOCD conjugates (Ch-TOCD 1:1, Ch-TOCD 1;2 and Ch-TOCD 3:1) by a) solid content: b) elemental analysis; and c) FTIR spectra.